International Journal of Biological Macromolecules 259 (2024) 129288

Contents lists available at ScienceDirect

International Journal of Biological Macromolecules

journal homepage: www.elsevier.com/locate/ijbiomac

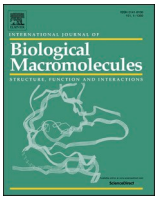

Resveratrol-loaded octenyl succinic anhydride modified starch emulsions and hydroxypropyl methylcellulose (HPMC) microparticles: Cytotoxicity and antioxidant bioactivity assessment after *in vitro* digestion

Pedro M. Silva [a,b,c], Mafalda D. Neto [c], Miguel A. Cerqueira [c], Isabel Rodriguez [c], Ana Isabel Bourbon [c], Ana Gabriela Azevedo [c], Lorenzo M. Pastrana [c], Manuel A. Coimbra [d], Antonio A. Vicente [a,b,*], Catarina Gonçalves [c]

[a] Centre of Biological Engineering (CEB), Campus de Gualtar, University of Minho, 4710-057 Braga, Portugal
[b] Associate Laboratory (LABBELS), Braga, Guimarães, Portugal
[c] International Iberian Nanotechnology Laboratory (INL), Av. Mestre José Veiga, 4715-330 Braga, Portugal
[d] LAQV/REQUIMTE, Department of Chemistry, University of Aveiro, 3810-193 Aveiro, Portugal

ARTICLE INFO

Keywords:
Gastrointestinal fate
Functional foods
Intracellular ROS
EHDP

ABSTRACT

Hydroxypropyl methylcellulose (HPMC)-based microparticles and modified starch emulsions (OSA-MS) were loaded with resveratrol and characterized regarding their physicochemical and thermal properties. Both delivery systems were subject to an *in vitro* gastrointestinal digestion to assess the bioaccessibility of resveratrol. In addition, cell-based studies were conducted after *in vitro* digestion and cytotoxicity and oxidative stress were assessed.

HPMC-based microparticles displayed higher average sizes (d) and lower polydispersity index (PDI) ($d = 948$ nm, PDI < 0.2) when compared to OSA-MS-based emulsions ($d = 217$ nm, PDI < 0.3). Both proved to protect resveratrol under digestive conditions, leading to an increase in bioaccessibility. Resveratrol-loaded HPMC-microparticles showed a higher bioaccessibility (56.7 %) than resveratrol-loaded emulsions (19.7 %).

Digested samples were tested in differentiated co-cultures of Caco-2 and HT29-MTX, aiming at assessing cytotoxicity and oxidative stress, and a lack of cytotoxicity was observed for all samples. Results displayed an increasing antioxidant activity, with 1.6-fold and 1.4-fold increases over the antioxidant activity of free resveratrol, for HPMC-microparticles and OSA-MS nanoemulsions, respectively.

Our results offer insight into physiological relevancy due to assessment post-digestion and highlight the protection that the use of micro-nano delivery systems can confer to resveratrol and their potential to be used as functional food ingredients capable of providing antioxidant benefits upon consumption.

1. Introduction

The use of functional ingredients has risen for the past couple of years. Market projections predict an increase of around 6 % over the next decade, reaching a market value of 120 to 160 billion US dollars [1–3]. This increase comes on the heels of increased consumer awareness of the effect of their eating habits [4–6].

Resveratrol is of interest due to its health-promoting properties, such as antioxidant, anti-inflammatory, anti-obesity, anti-diabetic, anti-carcinogenic, and antimicrobial [7–13].

Nonetheless, it presents low water solubility (~0.03 mg/L), chemical instability and it is vulnerable to degradation when added to food products [14–16]. Resveratrol can be degraded when subjected to external stimuli, as during *in vitro* digestion, losing part of its health-promoting properties and leading to a less efficient delivery due to low bioaccessibility. Additionally, resveratrol has a strong bitter taste, a challenge for its use in food products [15,17,18]. The potential health benefits of resveratrol combined with its disadvantages *e.g.* when using it for direct addition to foods, make it an ideal candidate for exploration of micro-nano encapsulation for the development of functional foods [99].

An emerging method in the production of delivery systems is

* Correspondence to: A. A. Vicente, Centre of Biological Engineering (CEB), Campus de Gualtar, University of Minho, 4710-057 Braga, Portugal.
E-mail address: avicente@deb.uminho.pt (A.A. Vicente).

https://doi.org/10.1016/j.ijbiomac.2024.129288
Received 28 September 2023; Received in revised form 18 December 2023; Accepted 4 January 2024
Available online 10 January 2024

electrohydrodynamic processing (EHDP). It makes use of voltage differences between a spinneret tip and a collector to evaporate the solvent of a solution and produce micro-nanostructures. It is an easy, one-step process that allows high encapsulation efficiency. It can be used with labile bioactives if conducted at room temperature [19]. Through fine-tuning of process parameters (*e.g.*, solution concentration, flow rate, voltage, and tip-to-collector distance), it is possible to control the morphology of the structures, with a low particle size and polydispersity index (PDI) and a high surface-area-to-volume ratio, as recently explored in the food research area [19–21,99]. The biggest disadvantage of this technology is its limited scale-up, although some solutions have been proposed to offset this issue, namely the use of multiple needle setups, and even the use of needle-less setups [22–24]. HPMC is one of many polymers (*e.g.*, Eudragit, cyclodextrin, among others) that have recently been explored for flavor masking applications, thus being of high interest for encapsulation of resveratrol [25].

Emulsification is one of the most used technologies in the food industry for the development of delivery systems. Typically, low-energy methods are more energy efficient and impart a lower exposure to temperature but may require high amounts of emulsifier. On the other hand, high-energy methods are more energy-costly and subject to high temperatures but can present advantages regarding the production of structures with low size and PDI. This results in advantages regarding emulsion stability against aggregation and improved emulsion transparency and less surfactant is needed when compared with low-energy methods [4,26,27]. Among emulsifiers, octenyl succinic anhydride-modified starch (OSA-MS) is reported to have flavor masking properties and as such can be an option to deal with the intense bitterness of resveratrol [28,29].

In vitro models of human digestion are used to evaluate the gastrointestinal fate of functional ingredients by mimicking physiological conditions following either static or more complex dynamic digestion methods [30–32,99]. Cell-based models (mono or co-cultures) are used to recapitulate the gut epithelium, allowing the assessment of cytotoxicity, production of reactive oxygen species (ROS), permeability, among other cellular responses. Few authors [33,34] have gathered studies of digestion of resveratrol-loaded structures, as well as, assessed cytotoxicity and bioactivity of those structures in cell-based models. There is currently a lack of research evaluating cellular responses after *in vitro* digestion, as reports are typically limited to evaluating non-digested samples.

The delivery of bioactive functional ingredients using different micro- or nanostructures determines its efficiency (bioaccessibility) and safety (cytotoxicity) during digestion. Then, conducting cell-based studies after *in vitro* digestion represents a more physiologically relevant scenario and should be encouraged, which was the main goal of this work. Additionally, this paper aims to compare the effect of different delivery systems on bioaccessibility, cytotoxicity, and *in vitro* antioxidant activity, comparing a well-established technology in the food industry, emulsification, *versus* an up-and-coming technology, electrohydrodynamic processing, that presents potential advantages regarding the use of heat sensitive bioactive compounds, such as resveratrol. Additionally, these two systems allow for a comparison between aqueous (EHDP) and lipidic (emulsions) delivery systems. To do this, resveratrol (RSV)- OSA-MS emulsions and hydroxypropyl methylcellulose (HPMC) microparticles were prepared, physiochemically and morphologically characterized, and digested following a harmonized static *in vitro* digestion protocol [30] to assess resveratrol bioaccessibility. After digestion, cellular responses were evaluated on a co-culture of differentiated Caco-2 and HT29-MTX cells assaying the potential cytotoxicity of the structures as we all as the induction of oxidative stress, and intracellular antioxidant activity of digested and non-digested formulations.

2. Materials and methods

2.1. Materials

Hydroxypropyl methylcellulose (HPMC 44779, HPMC LMW) (methoxyl 28–30 %, hydroxypropyl 7–12 %, viscosity 2 % aqueous solution, 20 °C, 40–60 mPa.s, 90 kDa) was purchased from Alfa Aesar GmbH & Co KG (Germany). Absolute ethanol (>99.8 %) was purchased from Honeywell (USA). Resveratrol (trans-resveratrol, 99 %, Bulk, Mirków, Poland); refined sunflower oil (100 % sunflower, Sovena, Portugal) (10 % saturated lipids, 42 % monounsaturated lipids and 39 % of polyunsaturated lipids); octenyl succinic anhydride modified starch (OSA-MS) (C*EmCap 12635, Cargill, Iowa, United States); distilled water, and ultrapure water type 1, generated by a Mili-Q system. Caco-2 HTB-37 cells were purchased from the American Type Culture Collection (ATCC®) and HT29-MTX-E12 cells from the European Collection of Authenticated Cell Cultures (ECACC 12040401). Minimum essential media (MEM) Eagle, Trypsin-EDTA (0.25 % trypsin; 0.1 % EDTA), and penicillin/streptomycin 100× were purchased from PAN-Biotech GmbH (Aidenbach, Germany). Foetal bovine serum (FBS) and Hank's balanced salt solution (HBSS) were bought from Merck Millipore (Burlington, MA, USA). Dimethyl sulfoxide (DMSO), paraformaldehyde (PFA), resazurin sodium salt, Dulbecco's modified Eagle's Medium-high glucose (DMEM), phosphate buffered saline (PBS), 2′,7′-Dichlorofluorescein diacetate (DCFH-DA), Pefabloc® SC, 3-morpholinosidnonimine (Sin-1, 5 μM), and 6-Hydroxy-2,5,7,8-tetramethylchromane-2-carboxylic acid (Trolox) were obtained from Sigma-Aldrich (St. Louis, MO, USA).

2.1.1. Production of OSA-MS emulsions

OSA-MS emulsions were prepared as *per* previous protocols [35]. OSA-MS was dissolved in Mili-Q ultrapure water, at a concentration of 1.5 % (*w/v*), at 45 °C for 30 min. Oil-to-water ratio was 5:95, and emulsions were prepared for a total volume of 50 mL. Resveratrol at a concentration of 7.5 mg/mL of emulsion was used. Increasing the resveratrol content led to the destabilization of the emulsion (data not shown). Emulsions were prepared at room temperature *via* high-speed homogenization using an Ultraturrax (T 25 digital Ultraturrax® disperser, IKA, Germany) at 14,000 rpm for a duration of 2 min followed by ultrasonic homogenization at a frequency of 20 kHz (Branson Digital Sonifier Model 450, Branson Ultrasonics Corporation, USA) using a 13 mm horn diameter, with a measured power output of 45 W, for a duration of 7 min, with pulsed intervals of 5 s "on" and 7 s "off", using a room temperature water bath to prevent sample overheating. Blank samples were also prepared, skipping the resveratrol dispersion step. Samples were frozen overnight at −80 °C and freeze-dried, at −50 °C and 1.0 mPa (LyoQuest −55 Plus, Telstar, Japan), until dry (between 48 h to 72 h) and stored in a light shielded container until use.

2.1.2. Production of HPMC microparticles

Polymer solutions were prepared as in Silva, Prieto, et al. [36,37] with slight modifications. Resveratrol was dissolved in pure ethanol for a final concentration of 0.75 mg/mL (2.5 % (*w*/w) loading), as higher concentrations led to morphology changes after EHDP (data not shown). Morphology changes due to increasing concentrations of bioactive compounds or drugs have been previously reported in other works [38–40]. Ultra-pure water was then added to a final concentration of 75 % (*v*/v) ethanol. Hydroxypropyl methylcellulose was then slowly added to the 75 % (v/v) ethanol solution to reach 3 % (*w/v*) and left to stir magnetically overnight at room temperature (~20 °C). After standing for a few hours to ensure air bubble removal, the HPMC solutions were ready to be used.

A Fluidnatek® LE-50 (Bioinicia, Valencia, Spain) was used to process the samples, equipped with a variable high voltage power supply (0–30 kV). Polymer solutions were electrosprayed under a steady flow rate using a blunt stainless-steel needle with an internal diameter of 0.601 mm (20G), connected to the syringe using a polytetrafluoroethylene

(PTFE) tube, with the flow rate controlled with a digitally controlled syringe pump (Bionicia S.L. Valencia, Spain). The temperature and relative humidity ranged between 20 °C and 25 °C and 45 % and 60 %, respectively for all experiments. Samples were processed at a flow rate of 500 μL/h, with a voltage of 10 kV, and a tip-to-collector distance of 15 cm. After processing, samples were stored in a parafilm-sealed Petri dish shielded from light. Blank samples were also prepared, skipping the resveratrol dissolution step.

2.2. Characterization of microparticles and emulsions

2.2.1. Morphology

A formulation of 3 % (*w/v*) low molecular weight HPMC was used for the microparticles production *via* EHDP, using a distance of 15 cm, a voltage of 10 kV, and a flow rate of 500 μL/h [36,37]. For the development of OSA nanoemulsions, 1.5 % (w/v) starch in a 95:5 water-to-oil ratio was used, as reported in previous works [35]. The RSV microparticles have a theoretical loading of 2.5 % (*w*/w), while the nanoemulsions have a loading of 13.3 % (w/w). The theoretical loading is calculated by dividing the amount of dried bioactive for the dried polymer.

Microparticles produced *via* EHDP were analysed by scanning electron morphology (SEM). Prior to analysis, samples were coated with gold under vacuum for 3 min (EM ACE200, Leica, Wetzlar, Germany) and subsequently characterized regarding their morphology using a scanning electron microscope (QUANTA 650FEG, FEI, Oregon, USA). 1–2 mg of sample were used for all SEM experiments. Diameter, aspect ratio, diameter distribution and aspect ratio distribution were measured using ImageJ software (v. 1.52a, Maryland, USA) as per Silva, Prieto, et al. [36]. Between 100 and 200 particles were measured.

Nanoemulsions morphology was analysed through transmission electron microscopy (TEM) (JEOL JEM 2100 - HT – 80-200 kV LaB6 gun, JEOL Ltd., Japan). The samples were loaded onto grids coated with an ultrathin carbon film (400 mesh, approx. grid hole size of 42 μm, PELCO®, TED PELLA INC., USA). As a contrast agent, UranyLess EM Stain (Electron Microscopy Sciences (EMS), USA) was used. The samples were left to dry at room temperature and after 24 h samples were imaged. The images were digitally recorded using an UltraScan® 4000 CCD camera (Oneview, Gatan, USA).

2.2.2. Size, PDI, and zeta potential

The droplet size, polydispersity (PDI), and zeta potential of the blank and loaded OSA-MS emulsions were characterized *via* DLS (Horiba SZ-100, Kyoto, Japan). Fresh samples were diluted (1:400) and analysed in DLS for a duration of 180 s, with three readings of three independently prepared samples. Size (by intensity) and PDI were obtained using a detection angle of 90°, while for the zeta potential a detection angle of 173° was used.

The stability of emulsions (measured by size, PDI, zeta potential) was analysed over a period of 3 months, with storage at room temperature and at 4 °C. Analysis were conducted every ~7 days and samples were stored in the dark.

2.2.3. Thermal analysis

Samples (*ca.* 5 mg) were placed and weighted in an alumina crucible in a thermogravimetric analyser (TGA/DSC STAR 1, Mettler Toledo, Ohio, USA). Temperature of analysis ranged 25 to 600 °C at a rate of 20 °C/min under a nitrogen atmosphere (flow rate: 70 mL/min). The weight loss, in percentage, and its derivative were represented as function of temperature. Data were calculated using Origin 9.0 software (OriginLab Corporation, 2012).

2.2.4. X-ray diffraction

An X-Ray Diffractometer X Pert PRO MRD system from Malvern Panalytical Ltd. (Royston, UK), was used to study the crystalline polymorphism of the micro- and nanostructures. Data was acquired at room temperature, using angular scans from 10° to 50° (2θ), performed with a Cu source, X-ray tube (λ = 1.54056 Å) at 45 kV and 40 mA (fine calibration offset for 2θ = −0.0372°). Data was collected for 174 s and Panalytical X'Pert HighScore Plus software was used to acquire and treat data.

2.2.5. ATR-Fourier transform infrared spectroscopy

Fourier Transform Infrared Spectroscopy (FTIR) was used to determine the functional groups and bonding arrangement of constituents present in samples. Sample analyses were carried out using an ALPHA II-Bruker spectrometer (Ettlingen, Germany) with a diamond-composite attenuated total reflectance (ATR) cell (range of 600–4000 cm^{-1}). 64 scans were used for each sample, with a resolution of 4 cm^{-1}. Analyses were conducted in triplicate using dry samples.

2.3. Resveratrol quantification

Resveratrol quantification was performed by HPLC using an Agilent 1200 series system (Agilent, Waldbronn, Germany) equipped with a Kinetex C18 100 Å, LC Column (150 × 4.6 mm, 2.6 μm, Phenomenex, USA) and a column guard system at 30 °C. The mobile phase was A: 1 mol/L acetic acid and B: acetonitrile:1 mol/L acetic acid (80:20). The compound was eluted and monitored at 306 nm using the following gradient: 18 % B for 10 min, 18–23 % B in 7 min, 23–31.5 % B in 10 min, 31.5–100 % B in 3 min, and finally 100 % A for 3 min. A 2 min post time was added between injections. The flow rate was 1.0 mL/min, and the injection volume was 20 μL. For calculation, area under the curve (AUC) was used for interpolation in a resveratrol (trans-resveratrol, 99 %, Bulk, Mirków, Poland) standard calibration curve ($Y = 145093X + 25.612$; $R^2 = 1$) prepared in methanol in the range 0.001–0.5 mg/mL.

2.4. Confocal scanning fluorescence microscopy (CLSM)

Samples were visualised using confocal scanning laser microscope (Zeiss LSM 780, Germany), with 20 × objective lens (Leica Microsystems,). Briefly, 100 μL sample were stained with 10 μL of a blended fluorescent colorant solution consisting of CalcoFluor White Stain (1 mg/mL) and Nile Red (1 mg/mL) for 15 min. CalcoFluor white-labelled starch was observed at an excitation wavelength of 405 nm. Using Nile red staining the oil-phase of emulsions were visualised at excitation wavelength of 514 nm. The optical resolution of the digital images was 1024 pixels × 1024 pixels.

2.5. In vitro digestion

The use of delivery systems for bioactives aims to provide them additional protection against oxidation or degradation in harsh conditions, such as those endured during food processing or gastrointestinal digestion.

The static INFOGEST protocol [30] was followed to determine the bioaccessibility of RSV-loaded in two different structures: HPMC microparticles (HPMC RSV) and emulsions (emulsion RSV). Additionally, free resveratrol (RSV), and distilled water were also digested to be used as controls.

The composition of the simulant fluids of each digestion phase can be found in Brodkorb et al. [30]. The activity of pepsin, used in the gastric phase, and of trypsin present in pancreatin, used in the intestinal phase, were quantified according to the procedure detailed in Brodkorb et al. [30]. The concentration of bile salts was tested using a commercial kit. The simulant fluids were prepared in advance and stored at −20 °C before use. The enzymes (pepsin and pancreatin) and bile salts were prepared just before each experiment to preserve activity and $CaCl_2$ was added just before each experiment to avoid precipitation. All incubations were carried out in a thermomixer (Eppendorf™, Hamburg, Germany).

As *per* the protocol simulant fluids [simulated salivary fluid (SSF), simulated gastric fluid (SGF), and simulated intestinal fluid (SIF)] were prepared 1.25 times concentrated, taking into consideration the dilution effect (4:1) along the digestive process. 1 mL of sample was prepared, ensuring that 4 mg of resveratrol were present. As such, 160 mg of HPMC particles were used, while for emulsions ~30 mg was taken, adding ultra-pure water up to 1 mL. The samples were vortexed for 30 s, and then for oral phase, 1 mL of sample was mixed up with 0.8 mL of SSF, 5.0 μL of 0.3 M $CaCl_2$, 100 μL of salivary amylase (75 U/mL final) and 95 μL of water to ensure a final volume of 2 mL. Samples were incubated at 37 °C for 2 min, at 500 rpm. For the gastric phase, the 2 mL of the oral phase (bolus) were mixed up with 1.6 mL of SGF, 100 μL of gastric lipase (RGE) (60 U/mL of gastric lipase and 2000 U/mL of pepsin in water), 1 μL of 0.3 mol/L $CaCl_2$. The pH was adjusted to 3.0 (using HCl 1 mol/L), water was added up to 4 mL and the mixture was incubated at 37 °C for 2 h, at 500 rpm.

The intestinal phase was prepared by adding to the gastric phase (chyme), 1.7 mL of SIF, 1.0 mL of pancreatin (100 U/mL final in SIF), 500 μL of bile salts (10 mmol/L in SIF), 8.0 μL of $CaCl_2$. The pH was adjusted to 7.0 (using NaOH 3 mol/L), water was added up to 8 mL and incubated at 37 °C for 2 h, at 500. To stop the intestinal digestion, 400 μL of Pefabloc® SC (0.1 mol/L in water) was added. Then, the samples were centrifuged at 3000 *g* for 20 min and the supernatant was collected and frozen. Resveratrol concentration in each digestion phase was determined by HPLC, after solvent extraction. The supernatant was extracted through solvent-solvent extraction. 1 mL of sample was added to 4 mL of methanol, vortexed for 1 min and placed in an ultrasound bath in pulse mode for 15 min. Samples were then centrifuged at 4 °C for 30 min, at 4000 *g*, and the supernatant was recovered and analysed in HPLC.

2.6. In vitro cellular assays

2.6.1. Sample preparation

Non-digested samples were homogenized in a vortex until complete dispersion, to ensure that flocculation does not happen on top of the cells during sample incubation with the cells. Vortex time varied between samples, with free resveratrol and emulsion samples taking the least amount of time, while HPMC samples took the longest (minimum 30 min). Digested samples were used as they were. Both digested and non-digested samples were diluted in HBSS (10 % *v*/v).

2.6.2. Cell cultures

Caco-2 and HT29-MTX cell lines were kept in a humidified chamber at 37 °C and 5 % CO_2. Culture media was changed every 2–3 days and cells were sub-cultured when reaching a confluence of 70–80 %. For cell detachment trypsin-EDTA (0.25 % trypsin; 0.1 % EDTA) was used for 5–10 min.

Caco-2 cells (passages 26–50) were cultured in MEM supplemented with 20 % foetal bovine serum (FBS), 100 U/mL of penicillin, and 100 μg/mL of streptomycin (1 % Pen/Strep).

HT29-MTX cells (passages 56–68) were maintained in DMEM medium supplemented with 10 % FBS and 1 % Pen/Strep.

2.6.3. Differentiated co-cultures of Caco-2 and HT29-MTX

Caco-2 and HT29-MTX cell lines were seeded at a 9:1 ratio, with a cell density of 1.0×10^5 cells/cm^2 in 96-well plates and incubated at 37 °C for 21 days to form a differentiated monolayer to carry out the assessment of cell viability and ROS production after incubation with samples.

2.6.4. Cell metabolic activity

Cytotoxicity of samples was determined indirectly by the resazurin reduction assay on differentiated monolayers of Caco-2:HT29-MTX (9:1 ratio) in 96-well plates. After 21 days of differentiation, culture media was removed and cells were incubated with samples for 4 h, and then samples were removed and resazurin solution (10 μg/mL in complete MEM) was added and incubated for 4 h. DMSO (40 %, *v*/v) was used as a negative control, HBSS with 10 % (*v*/v) dH_2O or HBSS with 10 % (v/v) digested dH_2O were used as positive control for non-digested or digested samples, respectively. To ensure that the simulant digestive fluids did not have any cytotoxicity, 1 mL of water was digested and diluted in HBSS, (10 %, v/v), then incubated for 4 h with cells, and the resazurin assay was conducted. Cells displayed no reduction in metabolic activity (Fig. 5), and as such the digested and non-digested samples were able to be analysed following the same conditions (1:10 dilution in HBSS, for 4 h).

Cell metabolic activity was determined through measurement of fluorescence intensity of the product of resazurin reduction - resorufin, which is proportional to the number of viable cells, using a microplate reader at $\lambda_{ex} = 560$ nm and $\lambda_{em} = 590$ nm (BioTek® Synergy H1, Winnoski, VT, USA). The % cell viability was expressed as the fluorescence of treated cells compared to the fluorescence of the positive control.

2.6.5. Intracellular ROS assessment

ROS are natural by-products of regular cell activity and essential signalling molecules [41]. However, an imbalance between oxidant external stimuli and anti-oxidant defence mechanisms, known as oxidative stress, can trigger cell damage and cause cell death [42].

Cell-based assays have been used to assess the effectiveness of dietary antioxidant compounds [43], quantifying the production of intracellular ROS using the oxidation sensitive 2′,7′-dichlorofluorescein diacetate (DCFH-DA), a cell-permeant and non-fluorescent molecule. After diffusion into the cell, DCFH-DA is deacetylated by cellular esterases, which is later oxidized into fluorescent DCF in the presence of ROS. When the basal level of intracellular ROS is increased, oxidative stress occurs [44]. Antioxidant compounds can quench this reaction and prevent the generation of DCF. HBSS with 10 % (*v*/v) dH_2O or HBSS with 10 % (v/v) digested dH_2O were used as negative control for non-digested or digested samples, respectively. Sin-1 (5 μmol/L), was used as positive control in the assessment of basal level of ROS or to induce inflammation in the assessment of protective effect. Trolox (50 μg/mL) was used as an antioxidant model.

2.6.5.1. Oxidative stress. ROS production was measured in the differentiated monolayer of Caco-2:HT29-MTX was assessed using DCFH-DA assay. After 21 days of differentiation, culture media was removed and replaced with 100 μL of 10 μmol/L of DCFH-DA diluted in HBSS. After 1 h, the DCFH-DA solution was replaced by 100 μL of samples diluted in HBSS (10 % v/v) and incubated for 4 h at 37 °C. After incubation, oxidative activity was determined by measuring dichlorofluorescein (DCF) fluorescence using a microplate reader at $\lambda_{ex} = 495$ nm and $\lambda_{em} = 525$ nm (BioTek® Synergy H1, Winnoski, VT, USA). Trolox (50 μg/mL), a known antioxidant, was used as a model compound and Sin-1 (5 μmol/L), a known oxidizer, was used as a positive control. Control wells were considered as the basal level of oxidation and results were calculated as a percentage relative to the respective control.

2.6.5.2. Protective effect. To investigate the potential protective effect of samples on intracellular ROS production (cellular antioxidant activity), after 4 h of incubation with samples, cells were stressed with Sin-1, 5 μmol/L for 60 min to induce oxidative stress. The fluorescence intensity of DCF was measured every 15 min throughout the 60 min, using a microplate reader at $\lambda_{ex} = 495$ nm and $\lambda_{em} = 525$ nm (BioTek® Synergy H1, Winnoski, VT, USA). Area under the curve was calculated for each sample, and results were expressed as percentage of protective effect increase over the negative controls (HBSS with 10 % (*v*/v) dH_2O for trolox and non-digested samples or HBSS with 10 % (v/v) digested dH_2O for digested samples).

2.7. Statistical analysis

Statistical analyses were completed using analysis of variance (ANOVA), Tukey's mean comparison test ($p < 0.05$), and students *t*-test ($p < 0.05$). Results are reported as an average and standard deviation. Origin 9.0 software (OriginLab Corporation, 2012) and GraphPad Prism 8.4.3 (GraphPad Software, LLC, 2020) were used. A minimum of 3 replicates were performed for the micro-nanostructure characterization. For the cellular assays, two individual experiments, each with 5 replicates, were performed.

3. Results and discussion

3.1. Morphology

The RSV microparticles have a theoretical loading of 2.5 % (*w*/w), while the nanoemulsions have a theoretical loading of 13.3 % (w/w). These loading capacities are in agreement with what has been previously reported for resveratrol micro-nano delivery systems (1 % to 20 % (w/w)) [45–48].

The morphology of the RSV-loaded HPMC microparticles produced by EHDP, and the starch nanoemulsions produced by high-speed homogenization and sonication can be found in Fig. 1.

The size of the RSV-loaded and unloaded microparticles and nanoemulsions were analysed *via* SEM and DLS, respectively, and results are presented in Table 1.

As shown in Fig. 1, microparticles produced *via* EHDP were round and smooth, with few uneven droplets formed during processing, with a low aspect ratio (indicating high sphericity). Most samples, both microparticles and nanoemulsions, displayed a PDI/diameter distribution lower than 0.3, indicating that they had a homogenous size distribution. The morphological parameters obtained for the HPMC microparticles produced *via* EHDP are similar to those previously reported in other works [49] [36,37].

In the case of nanoemulsions, they demonstrated a negative zeta potential. The negative value is indicative of the charge of the starch used to produce the emulsions, while the high value obtained (< -30 mV) can be an indicator of high stability [35,50].

Loading RSV in both structures did not influence their size. Regarding the HPMC microparticles, diameter distribution and span were slightly lower than what was reported in Silva, Prieto, et al. [36] (Table 1), likely due to the addition of resveratrol as it can modify solution properties such as viscosity or conductivity, similarly to what was seen in Silva, Prieto, et al. [36] upon the addition of melanoidins. Size and aspect ratio were similar. These results indicate that the HPMC microparticles produced in the specific conditions of these works can be a versatile system for the use of different bioactive compounds (at the tested loadings). Regarding the emulsions, it is shown in Table 1 that the addition of RSV, at a final loading of 7.5 mg RSV per mL of emulsion, did not create any significant differences between the loaded and unloaded systems, as size and PDI were similar.

The low size (< 1 μm) of the microparticles and emulsions present

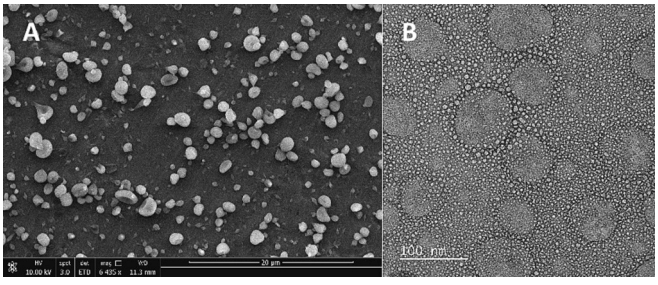

Fig. 1. SEM micrographs of the RSV loaded microparticles (A), TEM micrographs of nanoemulsions (B).

Table 1
Morphology parameters for the developed micro-nanostructures. *Data regarding the morphology of unloaded particles were also included for comparison [36,37]. [1]analysis *via* DLS, [2]analysis *via* SEM. Different letters in the same column represent statistically significant differences ($p < 0.05$).

Sample	Diameter (nm)	PDI/diameter distribution	Span	Aspect ratio	Zeta potential
RSV loaded HPMC particles[2]	948 ± 423[a]	0.20	1.2	1.32	–
Unloaded HPMC particles*[2]	919 ± 620[a]	0.46	2.1	1.26	–
RSV loaded OSA-MS emulsions[1]	217 ± 10[b]	0.27	–	–	−62.5
Unloaded OSA-MS emulsions[1]	227 ± 4[b]	0.27	–	–	−42.0

future advantages when projecting their use as a functional food ingredient, as size can be of influence regarding organoleptic properties such as mouthfeel and appearance, upon incorporation into food products [51–54].

3.2. Emulsion stability

The stability of the emulsions was assessed over a period of three months, at two storage temperatures: room (~23 °C) and cold storage (4 °C). This assessment was conducted using DLS, analysing the size, PDI (Fig. 2) and zeta potential (Fig. S1) of the loaded emulsions over time.

Loaded emulsions were stable for up to three months at both storage temperatures, with emulsions stored at room temperature destabilizing, regarding size and PDI, at the 88th day of storage. Cold stored samples display no statistically significant changes for size ($p > 0.05$), and while they displayed some statistically significant changes regarding PDI and zeta potential ($p < 0.05$), all the values are within the expected range. The maximum value recorded for PDI is 0.358 in day 21 and decreases over the next storage days to values below 0.3. Zeta potential reaches a minimum of −49.6 mV (Fig. S1), still well within the range of values considered to yield stable systems [50]. As for room temperature, emulsions destabilize at the 88th day, with the size increasing ($p < 0.05$) to an average value of 737.6 nm, compared to values that reached a maximum of 302.3 nm in the remaining time points. The same trend is seen for PDI, as all values for PDI are below 0.31, except for the 88th day, in which PDI sharply increases to 0.84 ($p < 0.05$)), indicating that the emulsions have destabilized. Instability in emulsions can be due to different factors, given the increase in both size and PDI value, it is likely to be either coalescence or Ostwald ripening mechanisms that are destabilizing the emulsions at room temperature storage [55,56].

Espinosa-Sandoval et al. [35] developed OSA stabilized Pickering emulsion for the delivery of essential oils through high-speed homogenization and ultrasonication and were able to maintain emulsion stability for a time-period of 14 days at cold (4 °C) and room temperature storage. Emulsion droplet size was ~150 nm, similar to our study.

3.3. Thermal and chemical characterization

3.3.1. TGA

Thermogravimetric analysis was conducted to understand the thermal properties of the produced structures, and whether the processing and the loading of RSV might influence their thermal properties.

Fig. S2 shows the thermograms of all analysed samples. Polymer raw materials and the respective structures display similar behaviours, indicating that processing did not influence the thermal properties of the produced structures. RSV displayed a one-stage degradation with an

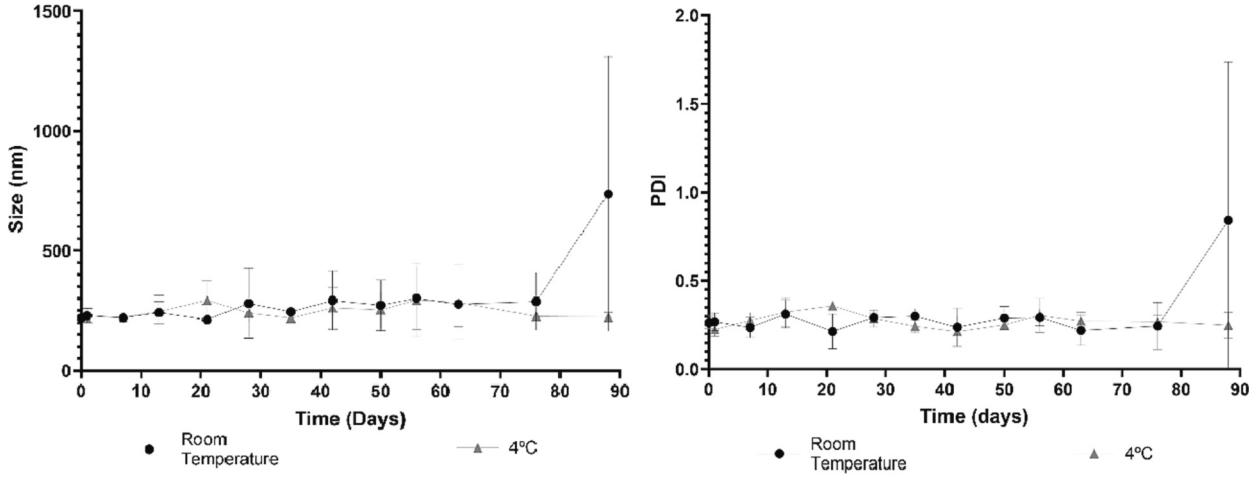

Fig. 2. Size (A) and polydispersity (B) stability at room and cold storage, over a period of three months.

onset temperature of ~250 °C and a peak temperature of ~350 °C and a final solid residue that accounts for ~36 % (*w*/w) of the initial sample weight.

For the EHDP produced structures, there is a single-stage degradation, starting at ~300 °C, likely to be due to cellulose ether degradation and dehydration and demethoxylation [57]. All HPMC lose around 80 % - 85 % (w/w) of their weight, ending with between 1 and 5 % (w/w) of their sample weight as a solid residue, with a maximum degradation peak between ~350 °C and ~ 375 °C.

These results follow what has been previously reported for HPMC particles [57,58] and RSV [45].

For OSA-MS and the resulting emulsions, data is slightly different. A single-stage degradation peak at ~300 °C was observed, with an onset temperature around 250 °C, accounting for ~70 % (w/w) of sample weight loss, with a final solid residue that accounts for ~4 % (w/w) of the initial sample weight. Blank emulsions display a two-stage degradation, possibly due to the presence of both polymer and oil. The first degradation stage initiates at ~200 °C, peaking at ~310 °C, accounting for a weight loss of 18 % (w/w), while the second degradation stage initiates ~345 °C, peaking at 425 °C, accounting for a weight loss of 74 % (w/w).

RSV emulsions display a similar behaviour, with slight shifts indicative of RSV incorporation. Samples display a two-stage degradation. The first stage initiates at ~200 °C, peaking at ~320 °C, accounting for ~16 % (w/w) of the initial weight loss, while the second stage starts at ~350 °C, peaking at ~420 °C, accounting for a weight loss of ~68 % (w/w), with a final solid residue of ~5 % (w/w). This two-stage degradation process is typical of starch emulsions, with the first degradation stage, with a peak around 300 °C, happening due to starch degradation, while the second degradation stage, peaking at around 420 °C, is due to the complete decomposition of starch-lipid complexes, as reported elsewhere [59].

Similar to what is seen with HPMC particles, the obtained results agree with what has been found in literature for starch [60] and starch emulsions [61] and RSV [45], regarding the weight loss profiles and temperature ranges at which they occur.

3.3.2. *X-ray diffraction*

X-ray diffraction analysis was carried out to assess the impact that the processing technologies (EHDP and emulsification) might have on the crystalline structure of HPMC and starch, and additionally explore how the use of an RSV delivery systems might affect its crystallographic profile. Supplementary Fig. S3 shows the spectra of all samples. HPMC display a mostly amorphous profile with one broad and low-intensity peak between 16° and 20°, peaking at 19.5° with a d-spacing of 4.55 Å, typical of HPMC [62,63]. The unloaded HPMC microparticles developed *via* EHDP display a lessening of this peak, indicating a lower crystallinity of materials. This decrease is typical of EHDP samples due to the rapid solidification of the stretched polymer chains during processing, and has been reported elsewhere [64,65]. Unloaded emulsions display a broad peak around 15° to 25°, peaking around 19°, typical of starch emulsions [66].

RSV presents a crystalline profile with several peaks in the 15° to 30° region, namely at 13.27°, 16.39°, 19.02°, 22.37°, 23.69° and 28.34°, characteristic of RSV and its crystalline structure [67,68].

Loaded RSV HPMC structures display similar features to the HPMC profile, with some additional low intensity peaks in regions typical of RSV, namely in the 20° to 30° region (20.21°, 20.55°, 22.62°, 25.73°, and 27.92°). These features are of low intensity given the low content of RSV in the microparticles, similar to what has been seen in other works using RSV delivery systems [68]. Loaded emulsions present a similar profile, but with the presence of additional peaks, likely due to the loading of resveratrol, as they appear in regions typical of resveratrol, as seen in the XRD profile of RSV. These peaks have a higher intensity than those seen in the loaded HPMC microparticles due to the higher RSV loading in OSA-MS emulsions. Nonetheless, when compared to the XRD profile of RSV, a decrease in the intensity of the peaks is still seen.

These results seem to indicate that RSV was successfully incorporated into the HPMC microparticles and nanoemulsions, and that the incorporation led to a decrease in the crystallinity of RSV, leading to its amorphization.

3.3.3. *ATR-FTIR*

ATR-FTIR analysis was conducted (Fig. S4) to assess the reorganization of any chemical and structural feature during processing or after RSV loading. FTIR band assignment is shown in Table S1. Supplementary Fig. S4 shows that pristine reagents displayed their typical profile (HPMC and starch) [69,70]. RSV also displayed its typical profile, with distinguishing features in the 1800–1500 cm^{-1} region [71,72].

Regarding processing, most samples were very similar among themselves, with only slight differences in their reagent controls. For example, there was a slight shift of the highest intensity peak of 1049 cm^{-1} for HPMC reagents to 1055 cm^{-1}, respectively, for the unloaded microparticles.

Upon the addition of RSV, there were only slight changes in the ATR-FTIR profile of the samples. Regarding the addition of RSV to the emulsions, it did not have a significant influence, as most of the peaks seen in these profiles are those typical of starch [97,98]. Nevertheless, in the region of 1600–1500 cm^{-1} a few additional peaks exist, typical of RSV, and of phenolic compounds in general [72,73]. Similar additional peaks are shown in the profile of the RSV-loaded HPMC particles in the regions of 1800–1700 cm^{-1} and 1600–1500 cm^{-1}. These peak shifts and

additions in both the loaded HPMC particles and the loaded emulsions are indicative that both micro-nanostructures were able to entrap RSV.

3.4. Simulated gastrointestinal digestive conditions

Fig. 3 shows the bioaccessibility of the different samples assayed with the INFOGEST protocol. Free resveratrol displayed the lowest bioaccessibility, with a value of 16.1 %. This can be due to two factors: 1) RSV is insoluble in water and, as such, might not be able to be micellized during the gastrointestinal digestion and therefore, is not bioaccessible; and 2) additionally, when dispersed in an aqueous phase, RSV is chemically unstable during gastrointestinal digestion. Combining the low water solubility and the high susceptibility to degradation under gastrointestinal conditions could leads to a low bioaccessibility after oral ingestion. Similar values were reported for other lipophilic polyphenolic compounds [74,75]. In the case of RSV, the intestinal conditions at higher pH have the highest impact on its stability and degradation [76].

Using delivery systems, the bioaccessibility of RSV increased (Fig. 3). HPMC RSV led to a higher increase in bioaccessibility, reaching a value of 56.7 %, while emulsion RSV increased to 19.7 %. In HPMC particles, resveratrol can be released through three different mechanisms: diffusion, swelling, and dissolution [77–80]. This leads to a more controlled, gradual, and slowed release of RSV in both, gastric and intestinal phases [77,78,80,81]. The slight increase, but still statistically different, in RSV bioaccessibility when loaded into the emulsions, may be due to the fast starch hydrolysis in the oral phase due to the amylase action, releasing the emulsified RSV faster than the HPMC RSV. The effect of amylase in the oral phase can be seen in Fig. 4. Before the addition of amylase, the oil is contained within the freeze-dried emulsion, and upon the addition of amylase, the freeze-dried emulsions are destabilized, and the oil and the starch are seen separately, resulting in the release of RSV.

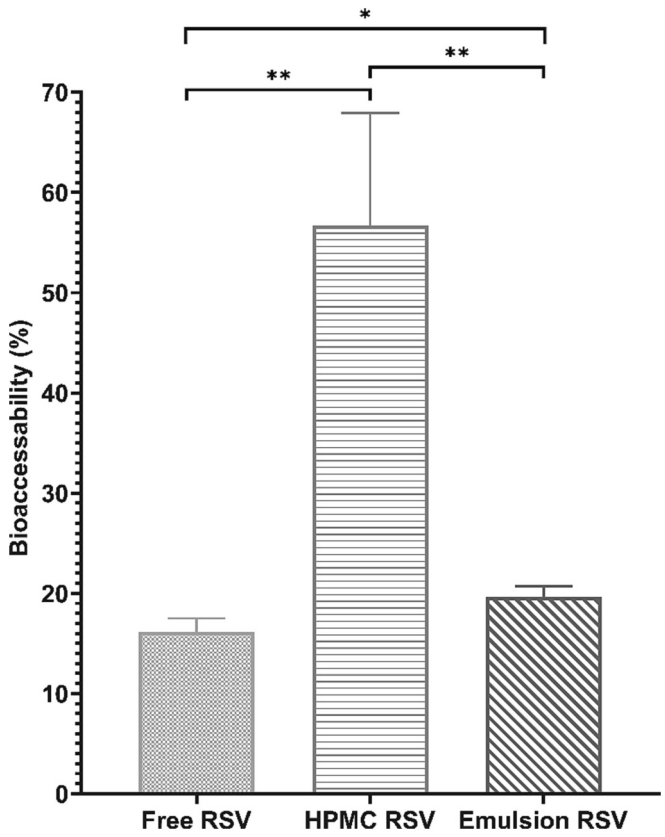

Fig. 3. Bioaccessibility of resveratrol after simulated gastrointestinal digestive conditions of resveratrol-loaded HPMC microparticles (HPMC RSV), resveratrol-loaded emulsions (Emulsion RSV), or free resveratrol (free RSV). The symbol (*) denotes significant differences (student *t*-test) between samples: ****$p < 0.0001$, ***$p < 0.001$; **$p < 0.01$, *$p < 0.05$.

A quicker release of RSV means that more RSV will be exposed to harsh gastrointestinal conditions, while a more controlled or slower release will result in higher protection, increasing bioaccessibility. This has been previously reported as one of the main advantages of the use of controlled delivery structures [82] and of possible interesting usage for RSV [83]. The bioaccessibility of the RSV emulsion was still higher than the free RSV. Despite the disintegration of the emulsion, the RSV might remain dispersed in oil droplets, making it slightly more stable, and thus more likely to be incorporated in mixed micelles, resulting in increased bioaccessibility [13,75]. Lipophilic polyphenolic compounds, such as resveratrol, usually degrade only in neutral and basic pH conditions, but can precipitate and sediment under acidic pH conditions [13,75]. As such, delaying the release of these compounds as far as possible can be beneficial, as seen by the results of the HPMC RSV formulation, which likely displayed a more sustained and gradual release of RSV.

Despite differences in magnitude similar trends, to what is observed here, are seen across different authors, with free RSV having a lower bioaccessibility than the delivery systems of RSV, regardless of the delivery system. Koga et al. [84] reported an increase in bioaccessibility from 23 % to 70–80 % for spray-dried RSV protein capsules, Jo et al. [85] reported an increase from 7 % to 90 % for emulsified RSV in chitosan-coated Pickering emulsions, and Pu, Tang, Liu, Zhu, & Sun [86] reported an increase from 14 % of bioaccessible RSV to a range between 44 and 72 % when RSV was encapsulated in kafirin. This further highlights the need and the advantages of using delivery systems for polyphenolic bioactive compounds, such as RSV.

A wide range of values are reported for bioaccessibility of RSV, either free or in a delivery system. Reports for the bioaccessibility of free RSV include values varying between 7 and 23 % [84,85]. Differences can be related to the lack of standardised protocols to simulate human gastrointestinal digestion. As an example, Koga et al. [84] use a protocol that recovers the micellar phase by centrifugation at 10,000 *g* for 60 min, while Jo et al. [85] centrifuge part of the digesta at 1500 *g* for 30 min, followed by a second centrifugation of the supernatant at 16,000 *g* for 20 min, followed by a dilution in methanol and centrifugation of 16,000 *g* for 20 min. Such differences in protocols over the different phases of the simulated digestion add up and can lead to differences in the outcome. As such, hampering a direct comparison of values might not be possible. Additionally, these differences highlight the need for a harmonized protocol for the simulation of the human digestion.

3.5. In vitro cellular assays

3.5.1. Cell metabolic activity

The assessment of the potential cytotoxic effect of new formulations using *in vitro* methodologies is essential to determine whether they are safe to consume without harming the host. Given the intended application of the developed formulations as functional food ingredients, it is essential to ensure their safety. It is of particular importance to test digested samples, representing what is effectively reaching the human intestine, thus providing a more physiologically relevant response. However, few studies using delivery systems of RSV have analysed the cell interactions with digested samples, while some have assessed the cytotoxicity of non-digested delivery systems [87–89]. As such, cell metabolic activity of a co-culture of Caco-2 and HT29-MTX (9:1 ratio) was assessed *via* the resazurin reduction assay after exposure to digested and non-digested samples.

Fig. 5 shows the cell viability (%) of differentiated co-culture of Caco-2 and HT29-MTX after 4 h of incubation with samples. The cell metabolic activity of the HBSS control samples was used as a baseline for 100 % cell viability for non-digested samples, while for digested samples, digested dH_2O was used. DMSO (40 % *v*/v), the negative control, displayed a cell viability of 38 %, demonstrating a cytotoxic effect, as expected.

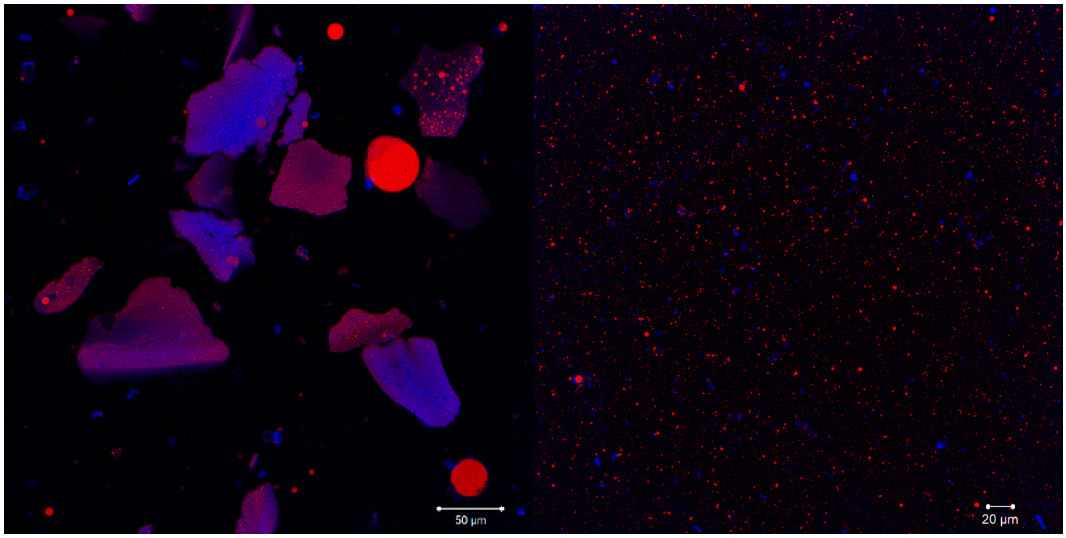

Fig. 4. Confocal microscopy image of freeze-dried emulsion in the simulated oral phase of the INFOGEST protocol, without (left) and with (right) amylase. Oil is stained with Nile red (shown in red) and starch is stained with calcofluor (shown in blue). (For interpretation of the references to colour in this figure legend, the reader is referred to the web version of this article.)

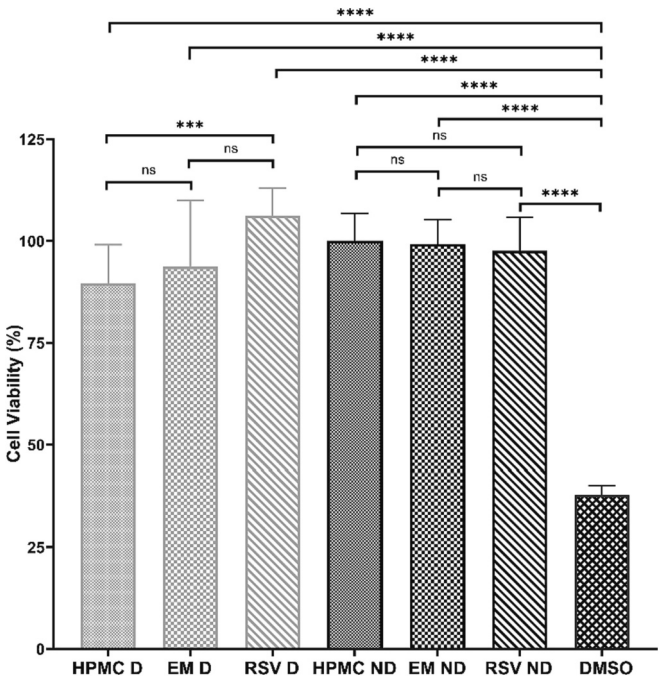

Fig. 5. Cell viability (%) of a differentiated co-culture of Caco-2 and HT29-MTX (9:1 ratio) after 4 h of incubation with samples, assessed by the resazurin assay. Electrosprayed HPMC RSV-loaded were analysed in their non-digested (HPMC ND) and digested form (HPMC D), as well as non-digested (EM ND) and digested (EM D) RSV loaded emulsions, and, non-digested (RSV ND) and digested (RSV D) free RSV. HBSS with 10 % (*v*/v), dH_2O or HBSS with 10 % (v/v) digested dH_2O were used as positive control for non-digested or digested samples, respectively and DMSO (40 % v/v) was used as negative control. All samples were prepared in HBSS (10 % v/v). The symbol (*) denotes significant differences (one-way ANOVA) between samples: ****$p < 0.0001$, ***$p < 0.001$; **$p < 0.01$, *$p < 0.05$.

All non-digested samples displayed a cell viability higher than 98 %, indicating that none of the samples compromised cellular metabolic activity. Similar results have been determined in other works, with Nunes et al. [87] developing RSV-loaded zein nanoparticles and reported cell viability higher than 80 %, usually with higher cell viability than free RSV. In another work, Qin, Zhao, et al. [89] developed RSV-loaded cellulose aerogels, with a cell viability higher than 90 %. Similarly, Qin, He et al. [88] developed RSV-loaded silica aerogels, and also reported a cell viability higher than 90 %.

Similar to the non-digested samples, the digested samples also displayed high values of cell viability, with all samples presenting values higher than 90 %.

There are only a few papers that evaluate the effect on cell-based models of delivery system after *in vitro* digestion. Huang et al. [49] digested zein and pectin core-shell nanoparticles loaded with RSV using the INFOGEST gastrointestinal model and reported that RSV displayed no cytotoxic effect, with cell viability above 80 %. In another work, Xu et al. [34] developed RSV-loaded liposomes and evaluated the *in vitro* cytotoxicity, after an *in vitro* gastrointestinal digestion [31]. Cell viability after incubation with all concentrations of free RSV was reported as higher than 85 %, while for the RSV-loaded liposomes it, was higher than 95 %.

3.5.2. Intracellular ROS assessment

3.5.2.1. Oxidative stress. As shown in Fig. 6a, Sin-1 effectively induced oxidative stress demonstrated by the increased intracellular level of ROS and, conversely, none of the analysed samples induced oxidative stress. Indeed, all samples decreased the basal intracellular level of ROS obtained in negative controls that were HBSS with 10 % (*v*/v) dH_2O or HBSS with 10 % (v/v) digested dH_2O for non-digested or digested samples, respectively, to similar or lower levels than the one observed for Trolox [90]. This result demonstrates the antioxidant effect (intracellular) of all formulations on the differentiated epithelial monolayer.

Non-digested HPMC RSV, free RSV, and emulsion RSV had a result of 67 %, 76 %, and 80 % of the fluorescence intensity of the basal level oxidation of the control, respectively. These results clearly indicate that most of the RSV was still within the microparticles and emulsion and, as such, could not actuate on cells, hence the lower reduction of the basal level of oxidation, when compared to a control (HBSS in sterile water). This is particularly true regarding the non-digested emulsion samples, given that they are easily dispersible and stable in water and as such likely had an extremely low release of RSV upon hydration from their freeze-dried form. As for free RSV, this result is likely due to oxidation or loss of RSV during the protocol, as it is unstable and insoluble in water.

All samples were ensured to be dispersed in water before incubation with cells, which meant dissolving the non-digested HPMC particles

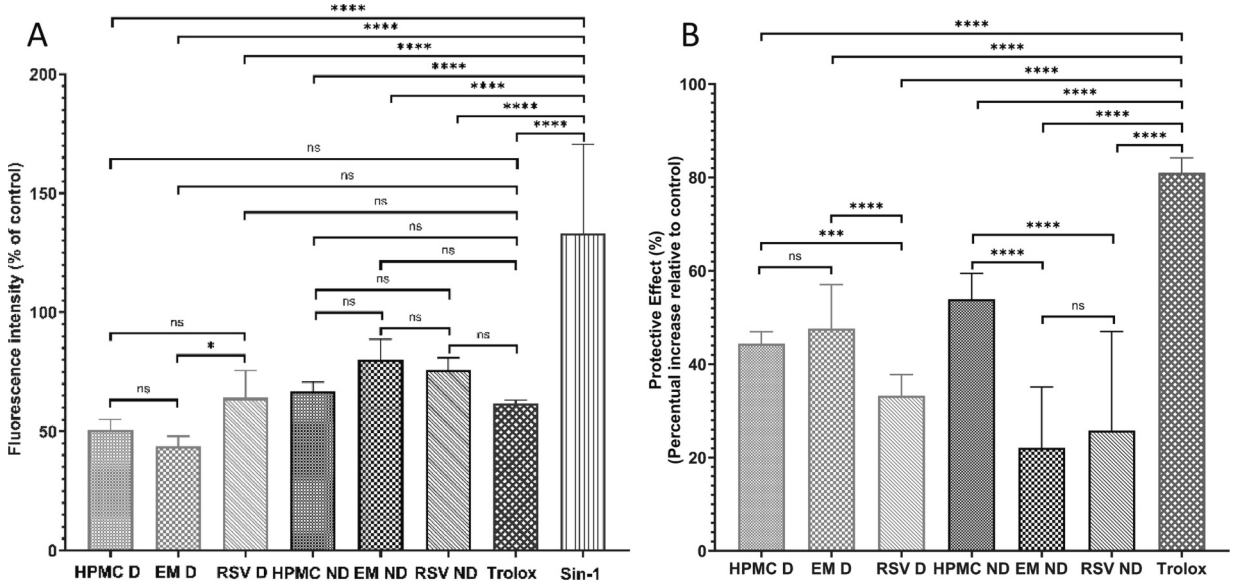

Fig. 6. Effect of samples on the basal level of ROS (a) and protective effect (b) on differentiated co-cultures of Caco-2 and HT29-MTX (9:1 ratio), after incubation for 4 h. Intracellular ROS was measured through the DCFH-DA assay (excitation 495 nm/emission 525 nm). HBSS with 10 % (v/v) dH_2O or HBSS with 10 % (v/v) digested dH_2O were used as negative control for non-digested or digested samples, respectively. Sin-1 (5 μmol/L), was used as the positive control in the assessing of basal level of ROS or to induce inflammation in the assessment of a protective effect. Trolox (50 μg/mL) was used as an antioxidant model. Values show mean ± sd (n = 8 from 2 independent assays). Electrosprayed HPMC RSV loaded were analysed in their non-digested (HPMC ND) and digested form (HPMC D), as well as non-digested (EM ND) and digested (EM D) RSV loaded emulsions, and, non-digested (RSV ND) and digested (RSV D) free RSV. The symbol (*) denotes significant differences (one-way ANOVA) between samples: ****$p < 0.0001$, ***$p < 0.001$; **$p < 0.01$, *$p < 0.05$.

before the incubation step of the protocol and then, samples were incubated with the cells for 4 h. The combination of these two factors might have led to some release of RSV, thus inducing the highest decrease when compared to the basal level of oxidation of the digested HBSS control when compared to the other non-digested samples.

Regarding the digested samples, it is clear the protection effect of the delivery system provides to RSV during digestion. For the emulsions (44 % of the basal level of oxidation of the control), the emulsified resveratrol resulted in a decrease of the basal level of oxidation when compared to the control, statistically different ($p < 0.05$) to the free digested RSV (64 % of the basal level of oxidation of the control). These results were similar to the HPMC digested samples (51 % of the basal level of oxidation of the control), and on par with the results achieved by Trolox (62 % of the basal level of oxidation of the control.

These results indicate that, when compared to the HBSS controls, none of the analysed samples resulted in any increase in the levels of intracellular ROS products, and samples were even able to reduce the basal level of ROS when compared to the control. These results also highlight one of the benefits of the use of delivery systems for sensitive bioactive compounds, as the protection conferred by it (namely for the emulsion) allowed for a higher decrease of the basal level of oxidation of the control, when compared to the free RSV sample.

3.5.2.2. Protective effect. The protective effect (antioxidant capacity) of samples was assessed by inducing oxidative stress with Sin-1 to cells after being in contact with samples (non-digested or digested samples) and controls. After oxidative stress induction, the area under the curve was calculated. Results are represented relative to controls: 10 % (v/v) distilled H_2O in HBSS for non-digested samples, 10 % (v/v) digestive fluids in HBSS for digested samples.

Fig. 6b shows that the non-digested samples had an even more distinctive behaviour among themselves. HPMC RSV displayed a high protective effect, while the non-digested emulsions barely presented any protective effect against oxidation, with a value of 22.1 %, similar to that of free RSV which displays a low protective effect of 25.8 %. While these values are similar, the reason behind them is likely to be different.

For the non-digested free RSV, the low protective effect is likely due to the insolubility of RSV in water, which might result in some degradation and loss of its antioxidant activity. As for the emulsions, given that they are easily dispersed in water upon rehydration, barely any RSV was likely released during the assays and, as such, it was unable to protect cells against oxidation. As seen in the stability tests, RSV-loaded emulsions were stable over a long period of time, indicating that no destabilization of the emulsions (and subsequent release of RSV) has occurred.

Regarding the non-digested sample of electrosprayed HPMC microparticles, a high protective effect against oxidation was verified, likely due to the controlled release of RSV from the HPMC microparticle. When in contact with water, the surface of HPMC particles hydrate and swell, forming a gel layer. The RSV will then gradually release over time from the HPMC microparticle, through various release mechanisms, including diffusion, swelling, and dissolution. As resveratrol is a poorly aqueous soluble bioactive, erosion is likely to be the dominant process [77–80]. As such, the probable increased and delayed release of RSV likely allowed it to maintain its stability, avoid degradation, and be available to act against oxidation, providing an increased protective effect (62.0 %) relative to the HBSS control.

Similar to what is shown in Fig. 6a, in the digested samples, the free RSV had significantly lower performance ($p < 0.05$) in terms of protective effect (33.3 %), than the digested RSV-loaded micro-nanostructures. This is likely due to the oxidation and degradation of RSV during the *in vitro* gastrointestinal digestion, decreasing RSV's ability to act against oxidation. Between the digested delivery systems, the protective effect was similar ($p > 0.05$), with the digested HPMC microparticles and digested emulsions having a protective effect increase of 44.4 % and 47.6 %, respectively, relative to the control of HBSS with digestive fluids. Trolox showed the highest protective effect relative to the HBSS control, with a protective effect increase over the control of 81.0 %.

The similarity of the protective effect of both the microparticles and nanoemulsions, despite the different bioaccessibilities seen in Fig. 3, can be explained by the different mechanisms of absorption of the different

systems. Nanoemulsions have a lower size than microparticles, which can facilitate absorption due to an increase in the adhesive contact between emulsions and the cellular membranes and a corresponding decrease in energy requirements for membrane deformation and cellular uptake [91,92]. Additionally, nanoemulsions have two pathways to cell internalization, micellization [93,94], and endocytosis [91], while polymeric microparticles do not undergo micellization, unless they have oil in their composition, which is not the case.

Over the past few years, some studies have analysed the antioxidant activity of RSV in cell culture, usually doing so with non-digested samples [95,96].

Chung et al. [95] developed two formulations of RSV-loaded chitosan–γ-poly(glutamic acid) nanoparticles and reported similar values to those obtained in this work and that both formulations of the encapsulated RSV had significantly higher cellular antioxidant activity values (CAA value) than the free RSV, reaching CAA values between 50 and 60, compared to a CAA value of 40 for free RSV (dissolved in ethanol).

Fan et al. [96] developed RSV loaded zein nanoparticle with bovine serum albumin-caffeic acid conjugate. Similarly, encapsulating RSV within the zein nanoparticles resulted in an increased antioxidant activity when compared to free RSV. Likewise, both authors argued that the encapsulation of RSV led to increased stability and solubility, resulting in higher antioxidant activities.

Regarding the assessment of the antioxidant activity of RSV after *in vitro* gastrointestinal digestion, there is a lack of research, with only a few papers assessing its antioxidant potential.

Huang et al. [49] developed RSV loaded zein and pectin core-shell nanoparticles and after using an *in vitro* gastrointestinal model, applied the digested samples to HepG2 cells grown for 24 h. The authors reported that the digesta of the zein nanoparticles exhibited superior antioxidant activity when compared to both the digestion of free RSV and the digestion of a physical mixture of RSV, zein, and pectin.

In another work, Xu et al. [34] applied the digesta of RSV-loaded liposomes to Caco-2 cells to investigate its antioxidant activity. Caco-2 cells were cultured for 4 h and samples were incubated with cells over a period of 24 h, followed by the antioxidant activity assay using the CellROX Deep Red assay. The authors assayed the encapsulated RSV and free RSV after digestion and reported that the encapsulated RSV decreased total fluorescence intensity of ROS production when compared to a control. Encapsulated RSV obtained 64.5 % of the total fluorescence intensity of the control, a significantly better result than the 78.4 % of the total fluorescence intensity of the control obtained for the free RSV.

Both authors point at the existence of a higher level of active RSV in the digesta fluid of the encapsulated RSV as the reason for the increased antioxidant activity, likely meaning that the encapsulated RSV displayed a higher stability (given the additional protection of encapsulation) to the *in vitro* gastrointestinal digestion and, as such, was able to be more active against oxidation. Despite the differences in the testing protocols between these works and the one presented in this paper, the result trends are in accordance, clearly indicating that the encapsulation and resulting stability provided to RSV led to an increased antioxidant activity.

All the analysed samples in this study were able to provide an increased protective effect relative to their sample controls, indicating the potential of RSV to be used as a functional food ingredient. This was especially true of both the digested delivery systems when compared to the free RSV.

RSV is considered to have a strong antioxidant capacity that is held back due to poor availability, resulting in low solubility and high susceptibility to oxidation and degradation. The differences in ROS levels shown between encapsulated and non-encapsulated samples can be mainly attributed to the encapsulation of RSV in the HPMC microparticles and starch emulsions, highlighting the benefits of encapsulating RSV as a protection mechanism against oxidation and degradation during *in vitro* gastrointestinal digestion.

4. Conclusions

The use of a delivery system improved the protection and bioaccessibility of RSV, in particular with the electrosprayed RSV-loaded HPMC microparticles presenting the best results, with a 3.5-fold increase, over the free resveratrol. All samples achieved a cell viability higher than 97 %, *vs* HBSS control. Regarding intracellular ROS production, all samples produced lower levels of ROS, namely the digested samples of the electrosprayed HPMC particles and the modified starch samples, similar to Trolox, a known antioxidant compound.

Regarding the protective effect against oxidative stress, RSV-loaded micro-nanostructures displayed a lower protective effect compared to Trolox, but still a significantly higher protective effect when compared to the controls used (HBSS), and most importantly to free resveratrol, highlighting the benefit of the use of a delivery system.

These results show the benefits of using nano or micro delivery systems as a way to add resveratrol to food products.

The HPMC-RSV-loaded microparticles could be added to dried foods as they would degrade in liquids, while the RSV-OSA-MS emulsions are extremely promising for use as a versatile functional ingredient, as they can be use in both liquid and dried form. Even with a low bioaccessibility, RSV-OSA-MS were able to increase the intracellular antioxidant activity when compared to free resveratrol, and as such should be further investigated as a potential functional food ingredient.

Supplementary data to this article can be found online at https://doi.org/10.1016/j.ijbiomac.2024.129288.

CRediT authorship contribution statement

Pedro M. Silva: Conceptualization, Formal analysis, Investigation, Methodology, Writing – original draft, Writing – review & editing. **Mafalda D. Neto:** Formal analysis, Investigation, Methodology, Writing – review & editing. **Miguel A. Cerqueira:** Conceptualization, Funding acquisition, Investigation, Methodology, Supervision, Writing – review & editing. **Isabel Rodriguez:** Formal analysis, Investigation, Methodology, Writing – review & editing. **Ana Isabel Bourbon:** Formal analysis, Investigation, Methodology, Writing – review & editing. **Ana Gabriela Azevedo:** Investigation, Methodology, Writing – review & editing. **Lorenzo M. Pastrana:** Conceptualization, Funding acquisition, Supervision, Writing – review & editing. **Manuel A. Coimbra:** Conceptualization, Funding acquisition, Supervision, Writing – review & editing. **Antonio A. Vicente:** Conceptualization, Funding acquisition, Supervision, Writing – review & editing. **Catarina Gonçalves:** Conceptualization, Formal analysis, Funding acquisition, Methodology, Supervision, Writing – review & editing.

Declaration of competing interest

The authors declare no conflict of interest.

Acknowledgements

This study was supported by the Portuguese Foundation for Science and Technology (FCT) under the scope of the strategic funding of UIDB/04469/2020 unit, and by LABBELS – Associate Laboratory in Biotechnology, Bioengineering and Microelectromechanical Systems, LA/P/0029/2020 and LAQV/REQUIMTE (UIDB/50006/2020, UIDP/50006/2020). This work was funded by the SbDtoolBox - Nanotechnology-based tools and tests for Safer-by-Design nanomaterials, with the reference NORTE-01-0145-FEDER-000047, funded by Norte 2020 – North-Regional Operational Program under the PORTUGAL 2020 Partnership Agreement, through the European Regional Development Fund (ERDF). The research also received funding from the European Union's H2020 research and innovation program under the Marie Sklodowska-

Curie grant agreement N 778388 (H2020 MSCA-RISE-2017 project Food for Diabetes and Cognition (FODIAC), and grant agreement N 713640 (MSCA-2015-COFUND-FP). Pedro Silva is the recipient of a fellowship (SFRD/BD/130247/2017) supported by Fundação para a Ciência e a Tecnologia, (FCT, Portugal). Ana Isabel Bourbon acknowledges funding by FCT, through the individual scientific employment program contract (2020.03447.CEECIND). We also would like to thank the Advanced Electron Microscopy, Imaging, and Spectroscopy (AEMIS) and the Nanophotonics and Bioimaging Facility (NBI) from INL for their support.

References

[1] Grand View Research, Global Specialty Food Ingredients Market Size Report 2030, 2022. https://www.grandviewresearch.com/industry-analysis/specialty-food-ingredients-market.
[2] Markets and Markets, Speciality Food Ingredients Market Forecast 2022-2027 | Industry Size, Share, Growth Trends. https://www.marketsandmarkets.com/Market-Reports/speciality-food-ingredients-market-252775011.html, 2022.
[3] The Business Research Company, Specialty Food Ingredients Market Analysis, Size And Trends Forecast To 2022-2030. https://www.thebusinessresearchcompany.com/press-release/specialty-food-ingredients-market-2022, 2022.
[4] S.F. Hosseini, L. Ramezanzade, D.J. McClements, Recent advances in nanoencapsulation of hydrophobic marine bioactives: bioavailability, safety, and sensory attributes of nano-fortified functional foods, Trends Food Sci. Technol. 109 (2021) 322–339, https://doi.org/10.1016/j.tifs.2021.01.045.
[5] H. Koc, C.J. Vinyard, G.K. Essick, E.A. Foegeding, Food oral processing: conversion of food structure to textural perception, Annu. Rev. Food Sci. Technol. 4 (1) (2013) 237–266, https://doi.org/10.1146/annurev-food-030212-182637.
[6] F. Temelli, Perspectives on the use of supercritical particle formation technologies for food ingredients, J. Supercrit. Fluids 134 (2018) 244–251, https://doi.org/10.1016/j.supflu.2017.11.010.
[7] T.T. Cai, X.L. Ye, R.R. Li, H. Chen, Y.Y. Wang, H.J. Yong, M.L. Pan, W. Lu, Y. Tang, H. Miao, A.M. Snijders, J.H. Mao, X.Y. Liu, Y.B. Lu, D.F. Ding, Resveratrol modulates the gut microbiota and inflammation to protect against diabetic nephropathy in mice, Front. Pharmacol. 11 (2020) 1249, https://doi.org/10.3389/fphar.2020.01249.
[8] A. Davoodvandi, M. Darvish, S. Borran, M. Nejati, S. Mazaheri, O. Reza Tamtaji, M. R. Hamblin, N. Masoudian, H. Mirzaei, The therapeutic potential of resveratrol in a mouse model of melanoma lung metastasis, Int. Immunopharmacol. 88 (2020) 106905, https://doi.org/10.1016/j.intimp.2020.106905.
[9] M. Shabani, A. Sadeghi, H. Hosseini, M. Teimouri, R. Babaei Khorzoughi, P. Pasalar, R. Meshkani, Resveratrol alleviates obesity-induced skeletal muscle inflammation via decreasing M1 macrophage polarization and increasing the regulatory T cell population, Sci. Rep. 10 (1) (2020) 1–13, https://doi.org/10.1038/s41598-020-60185-1.
[10] R. Torregrosa-Muñumer, E. Vara, J.Á. Fernández-Tresguerres, R. Gredilla, Resveratrol supplementation at old age reverts changes associated with aging in inflammatory, oxidative and apoptotic markers in rat heart, Eur. J. Nutr. 1–11 (2021), https://doi.org/10.1007/s00394-020-02457-0.
[11] K. Wang, Z. Chen, J. Shi, Y. Feng, M. Yu, Y. Sun, Q. Zhuang, B. Liang, G. Luo, X. Xu, M. Fan, Resveratrol inhibits the tumor migration and invasion by upregulating TET1 and reducing TIMP2/3 methylation in prostate carcinoma cells, Prostate 80 (12) (2020) 977–985, https://doi.org/10.1002/pros.24029.
[12] P. Wang, J. Gao, W. Ke, J. Wang, D. Li, R. Liu, Y. Jia, X. Wang, X. Chen, F. Chen, X. Hu, Resveratrol reduces obesity in high-fat diet-fed mice via modulating the composition and metabolic function of the gut microbiota, Free Radic. Biol. Med. 156 (2020) 83–98, https://doi.org/10.1016/j.freeradbiomed.2020.04.013.
[13] H. Zhou, B. Zheng, D.J. Mcclements, In vitro gastrointestinal stability of lipophilic polyphenols is dependent on their oil-water partitioning in emulsions: studies on curcumin, resveratrol, and quercetin, J. Agric. Food Chem. 69 (11) (2021) 3340–3350, https://doi.org/10.1021/acs.jafc.0c07578.
[14] M. Chávarri, M.C. Villarán, Encapsulation technologies for resveratrol in functional food, in: J. Ruiz, M. Campos (Eds.), New Polymers for Encapsulation of Nutraceutical Compounds, John Wiley & Sons, Ltd., 2017, pp. 159–194, https://doi.org/10.1002/9781119227625.ch8.
[15] G. Davidov-Pardo, D.J. McClements, Resveratrol encapsulation: designing delivery systems to overcome solubility, stability and bioavailability issues, Trends Food Sci. Technol. 38 (2) (2014) 88–103, https://doi.org/10.1016/j.tifs.2014.05.003.
[16] B.V. Fiod Riccio, B. Fonseca-Santos, P. Colerato Ferrari, M. Chorilli, Characteristics, biological properties and analytical methods of trans-resveratrol: A review, Crit. Rev. Anal. Chem. 50 (4) (2020) 339–358, https://doi.org/10.1080/10408347.2019.1637242.
[17] I. Lesschaeve, A.C. Noble, Polyphenols: factors influencing their sensory properties and their effects on food and beverage preferences, Am. J. Clin. Nutr. 81 (1 Suppl) (2005) 330S–335S, https://doi.org/10.1093/ajcn/81.1.330s.
[18] D.D. Torrico, S. Fuentes, C. Gonzalez Viejo, H. Ashman, F.R. Dunshea, Cross-cultural effects of food product familiarity on sensory acceptability and non-invasive physiological responses of consumers, Food Res. Int. 115 (2019) 439–450, https://doi.org/10.1016/j.foodres.2018.10.054.
[19] P.M. Silva, S. Torres-Giner, A.A. Vicente, M.A. Cerqueira, Electrohydrodynamic processing for the production of zein-based micro- and nanostructures, Curr. Opin. Colloid Interface Sci. (2021) 101504, https://doi.org/10.1016/j.cocis.2021.101504.
[20] J.L. Guía-García, A.V. Charles-Rodríguez, P. Silva, A. Robledo-Olivo, M. A. Cerqueira, M.L. Flores-López, Electrosprayed hydroxypropyl methylcellulose microcapsules containing Rhus microphylla fruit extracts and their application in strawberry (Fragaria × ananassa) preservation, LWT 184 (2023) 115048, https://doi.org/10.1016/j.lwt.2023.115048.
[21] P.M. Silva, S. Torres-Giner, A.A. Vicente, M.A. Cerqueira, Management of operational parameters and novel spinneret configurations for the electrohydrodynamic processing of functional polymers, Macromol. Mater. Eng. (2022) 2100858, https://doi.org/10.1002/mame.202100858.
[22] Bionicia, Bioinicia | Electrospinning & Electrospraying Equipment. https://bioinicia.com/capsultek/, 2022.
[23] M. Parhizkar, P.J.T. Reardon, J.C. Knowles, R.J. Browning, E. Stride, R.B. Pedley, T. Grego, M. Edirisinghe, Performance of novel high throughput multi electrospray systems for forming of polymeric micro/nanoparticles, Mater. Des. 126 (2017) 73–84, https://doi.org/10.1016/j.matdes.2017.04.029.
[24] P. Ryšánek, O. Benada, J. Tokarský, M. Syrový, P. Čapková, J. Pavlík, Specific structure, morphology, and properties of polyacrylonitrile (PAN) membranes prepared by needleless electrospinning; forming hollow fibers, Mater. Sci. Eng. C 105 (2019) 110151, https://doi.org/10.1016/j.msec.2019.110151.
[25] H. Sohi, Y. Sultana, R.K. Khar, Taste masking technologies in oral pharmaceuticals: recent developments and approaches, Drug Dev. Ind. Pharm. 30 (5) (2004) 429–448, https://doi.org/10.1081/DDC-120037477.
[26] J.S. Komaiko, D.J. McClements, Formation of food-grade Nanoemulsions using low-energy preparation methods: A review of available methods, Compr. Rev. Food Sci. Food Saf. 15 (2) (2016) 331–352, https://doi.org/10.1111/1541-4337.12189.
[27] A.M. Marques, M.A. Azevedo, J.A. Teixeira, L.M. Pastrana, C. Gonçalves, M. A. Cerqueira, Engineered nanostructures for enrichment and fortification of foods, in: Food Applications of Nanotechnology, CRC Press, 2019, pp. 61–97, https://doi.org/10.1201/9780429297038-4.
[28] Cargill, C*EmCap emulsifying starch | Cargill Food Ingredients EMEA | Cargill. https://www.cargill.com/food-bev/emea/starches-derivatives/c*emcap, 2023.
[29] A. Mirzapour-Kouhdasht, D.J. McClements, M.S. Taghizadeh, A. Niazi, M. Garcia-Vaquero, Strategies for oral delivery of bioactive peptides with focus on debittering and masking, Npj Science of Food 7 (1) (2023) 1–20, https://doi.org/10.1038/s41538-023-00198-y.
[30] A. Brodkorb, L. Egger, M. Alminger, P. Alvito, R. Assunção, S. Ballance, T. Bohn, C. Bourlieu-Lacanal, R. Boutrou, F. Carrière, A. Clemente, M. Corredig, D. Dupont, C. Dufour, C. Edwards, M. Golding, S. Karakaya, B. Kirkhus, S. Le Feunteun, I. Recio, INFOGEST static in vitro simulation of gastrointestinal food digestion, Nat. Protoc. 14 (4) (2019) 991–1014, https://doi.org/10.1038/s41596-018-0119-1.
[31] M. Minekus, M. Alminger, P. Alvito, S. Ballance, T. Bohn, C. Bourlieu, F. Carrière, R. Boutrou, M. Corredig, D. Dupont, C. Dufour, L. Egger, M. Golding, S. Karakaya, B. Kirkhus, S. Le Feunteun, U. Lesmes, A. MacIerzanka, A. MacKie, A. Brodkorb, A standardised static in vitro digestion method suitable for food-an international consensus, Food Funct. 5 (6) (2014) 1113–1124, https://doi.org/10.1039/c3fo60702j.
[32] A.I. Mulet-Cabero, L. Egger, R. Portmann, O. Ménard, S. Marze, M. Minekus, S. Le Feunteun, A. Sarkar, M.M.L. Grundy, F. Carrière, M. Golding, D. Dupont, I. Recio, A. Brodkorb, A. Mackie, A standardised semi-dynamic: in vitro digestion method suitable for food-an international consensus, Food Funct. 11 (2) (2020) 1702–1720, https://doi.org/10.1039/c9fo01293a.
[33] X. Huang, Y. Liu, Y. Zou, X. Liang, Y. Peng, D.J. McClements, K. Hu, Encapsulation of resveratrol in zein/pectin core-shell nanoparticles: stability, bioaccessibility, and antioxidant capacity after simulated gastrointestinal digestion, Food Hydrocoll. 93 (December 2018) (2019) 261–269, https://doi.org/10.1016/j.foodhyd.2019.02.039.
[34] X. Xu, M. Tian, L. Deng, H. Jiang, J. Han, C. Zhen, L. Huang, W. Liu, Structural degradation and uptake of resveratrol-encapsulated liposomes using an in vitro digestion combined with Caco-2 cell absorption model, Food Chem. 403 (2023) 133943, https://doi.org/10.1016/j.foodchem.2022.133943.
[35] L. Espinosa-Sandoval, C. Ochoa-Martínez, A. Ayala-Aponte, L. Pastrana, C. Gonçalves, M.A. Cerqueira, Polysaccharide-based multilayer nano-emulsions loaded with oregano oil: production, characterization, and in vitro digestion assessment, Nanomaterials 11 (4) (2021) 878, https://doi.org/10.3390/nano11040878.
[36] P.M. Silva, C. Prieto, C.C.P. Andrade, J.M. Lagarón, L.M. Pastrana, M.A. Coimbra, A.A. Vicente, M.A. Cerqueira, Hydroxypropyl methylcellulose-based micro- and nanostructures for encapsulation of melanoidins: effect of electrohydrodynamic processing variables on morphological and physicochemical properties, Int. J. Biol. Macromol. 202 (2022) 453–467, https://doi.org/10.1016/j.ijbiomac.2022.01.019.
[37] P.M. Silva, C. Prieto, J.M. Lagarón, L.M. Pastrana, M.A. Coimbra, A.A. Vicente, M. A. Cerqueira, Food-grade hydroxypropyl methylcellulose-based formulations for electrohydrodynamic processing: part I – role of solution parameters on fibre and particle production, Food Hydrocoll. (2021) 106761, https://doi.org/10.1016/j.foodhyd.2021.106761.
[38] S.C. Coelho, A. Giron, F. Rocha, B.N. Estevinho, Electrosprayed B-complex vitamins/zein microparticles for drug sustained release and antioxidant applications, J. Chem. Technol. Biotechnol. (2023), https://doi.org/10.1002/jctb.7526.
[39] Z. Mai, J. Chen, T. He, Y. Hu, X. Dong, H. Zhang, W. Huang, F. Ko, W. Zhou, Electrospray biodegradable microcapsules loaded with curcumin for drug delivery systems with high bioactivity, RSC Adv. 7 (3) (2017) 1724–1734, https://doi.org/10.1039/c6ra25314h.

[40] L. Mayol, A. Borzacchiello, V. Guarino, C. Serri, M. Biondi, L. Ambrosio, Design of electrospayed non-spherical poly (l-lactide-co-glicolide) microdevices for sustained drug delivery, J. Mater. Sci. Mater. Med. 25 (2) (2014) 383–390, https://doi.org/10.1007/s10856-013-5080-5.
[41] J. Zhang, X. Wang, V. Vikash, Q. Ye, D. Wu, Y. Liu, W. Dong, ROS and ROS-mediated cellular signaling, Oxidative Med. Cell. Longev. 2016 (2016), https://doi.org/10.1155/2016/4350965.
[42] A.A. Alfadda, R.M. Sallam, Reactive oxygen species in health and disease, J. Biomed. Biotechnol. 2012 (2012), https://doi.org/10.1155/2012/936486.
[43] M.E. Kellett, P. Greenspan, R.B. Pegg, Modification of the cellular antioxidant activity (CAA) assay to study phenolic antioxidants in a Caco-2 cell line, Food Chem. 244 (2018) 359–363, https://doi.org/10.1016/j.foodchem.2017.10.035.
[44] M. Marimoutou, F. Le Sage, J. Smadja, C.L. D'Hellencourt, M.P. Gonthier, C.R. Da Silva, Antioxidant polyphenol-rich extracts from the medicinal plants Antirhea borbonica, Doratoxylon apetalum and Gouania mauritiana protect 3T3-L1 preadipocytes against H2O2, TNFα and LPS inflammatory mediators by regulating the expression of superoxide dismut, Journal of Inflammation (United Kingdom) 12 (1) (2015), https://doi.org/10.1186/s12950-015-0055-6.
[45] A. Celebioglu, D. Tekant, M.E. Kilic, E. Durgun, T. Uyar, Orally fast-disintegrating resveratrol/cyclodextrin nanofibrous films as a potential antioxidant dietary supplement, ACS Food Science and Technology 2 (2021) 580, https://doi.org/10.1021/acsfoodscitech.1c00456.
[46] L. Consoli, M.D. Hubinger, M.M. Dragosavac, Encapsulation of resveratrol via spray-drying of oil-in-water emulsions produced by ultrasound or membrane emulsification, J. Food Eng. 350 (2023) 111488, https://doi.org/10.1016/j.jfoodeng.2023.111488.
[47] M. Maria Leena, K.S. Yoha, J.A. Moses, C. Anandharamakrishnan, Edible coating with resveratrol loaded electrospun zein nanofibers with enhanced bioaccessibility, Food Biosci. 36 (October 2019) (2020) 100669, https://doi.org/10.1016/j.fbio.2020.100669.
[48] B.G. Seethu, H.A. Pushpadass, F.M.E. Emerald, B.S. Nath, N.L. Naik, K. S. Subramanian, Electrohydrodynamic encapsulation of resveratrol using food-grade Nanofibres: process optimization, characterization and fortification, Food Bioprocess Technol. 13 (2) (2020) 341–354, https://doi.org/10.1007/s11947-019-02399-4.
[49] W. Huang, Y. Hou, X. Lu, Z. Gong, Y. Yang, X.J. Lu, X.L. Liu, D.G. Yu, The process–property–performance relationship of medicated nanoparticles prepared by modified coaxial electrospraying, Pharmaceutics 11 (5) (2019) 226, https://doi.org/10.3390/pharmaceutics11050226.
[50] S. Bhattacharjee, DLS and zeta potential - what they are and what they are not? J. Control. Release 235 (2016) 337–351, https://doi.org/10.1016/j.jconrel.2016.06.017.
[51] S. Beckett, Controlling the flow properties of liquid chocolate, in: The Science of Chocolate, Royal Society of Chemistry, 2008, https://doi.org/10.1039/9781847558053.
[52] E. Imai, K. Hatae, A. Shimada, Oral perception of grittiness: effect of particle size and concentration of the dispersed particles and the dispersion medium, J. Texture Stud. 26 (5) (1995) 561–576, https://doi.org/10.1111/j.1745-4603.1995.tb00804.x.
[53] E. Imai, Y. Shimichi, I. Maruyama, A. Inoue, S. Ogawa, K. Hatae, A. Shimada, Perception of grittiness in an oil-in-water emulsion, J. Texture Stud. 28 (3) (1997) 257–272, https://doi.org/10.1111/j.1745-4603.1997.tb00116.x.
[54] K. Petersson, A.C. Eliasson, E. Tornberg, B. Bergenståhl, Sensory perception of Rye bran particles of varying size and concentration in a viscous phase, J. Texture Stud. 44 (6) (2013) 459–467, https://doi.org/10.1111/jtxs.12034.
[55] B. Biduski, D.H. Kringel, R. Colussi, H.C. dos S Hackbart, L.T. Lim, A.R.G. Dias, E. da R Zavareze, Electrosprayed octenyl succinic anhydride starch capsules for rosemary essential oil encapsulation, Int. J. Biol. Macromol. 132 (2019) 300–307, https://doi.org/10.1016/j.ijbiomac.2019.03.203.
[56] H.A. Fonseca-Florido, H.G. Vázquez-García, G. Méndez-Montealvo, U.A. Basilio-Cortés, R. Navarro-Cortés, M.L. Rodríguez-Marín, J. Castro-Rosas, C.A. Gómez-Aldapa, Effect of acid hydrolysis and OSA esterification of waxy cassava starch on emulsifying properties in Pickering-type emulsions, LWT 91 (2018) 258–264, https://doi.org/10.1016/j.lwt.2018.01.057.
[57] A. Aydogdu, G. Sumnu, S. Sahin, A novel electrospun hydroxypropyl methylcellulose/polyethylene oxide blend nanofibers: morphology and physicochemical properties, Carbohydr. Polym. 181 (2018) 234–246, https://doi.org/10.1016/j.carbpol.2017.10.071.
[58] B. Mahesh, D. Kathyayani, G.S. Nanjundaswamy, D. Channe Gowda, R. Sridhar, Miscibility studies of plastic-mimetic polypeptide with hydroxypropylmethylcellulose blends and generation of non-woven fabrics, Carbohydr. Polym. 212 (2019) 129–141, https://doi.org/10.1016/j.carbpol.2019.02.042.
[59] W. Gao, J. Zhu, P. Liu, B. Cui, A.M. Abd El-Aty, Preparation and characterization of octenyl succinylated starch microgels via a water-in-oil (W/O) inverse microemulsion process for loading and releasing epigallocatechin gallate, Food Chem. 355 (December 2020) (2021) 129661, https://doi.org/10.1016/j.foodchem.2021.129661.
[60] D. Li, X. Zhang, Y. Tian, Ionic liquids as novel solvents for biosynthesis of octenyl succinic anhydride-modified waxy maize starch, Int. J. Biol. Macromol. 86 (2016) 119–125, https://doi.org/10.1016/j.ijbiomac.2016.01.050.
[61] J. Mou, X. Li, H. Wang, G. Fei, Q. Liu, Preparation, characterization, and water resistance of cationic acetylated starch-g-poly(styrene-butyl acrylate) surfactant-free emulsion, Starch/Staerke 64 (10) (2012) 826–834, https://doi.org/10.1002/star.201200041.
[62] H. Kadry, T.A. Al-Hilal, A. Keshavarz, F. Alam, C. Xu, A. Joy, F. Ahsan, Multi-purposable filaments of HPMC for 3D printing of medications with tailored drug release and timed-absorption, Int. J. Pharm. 544 (1) (2018) 285–296, https://doi.org/10.1016/j.ijpharm.2018.04.010.
[63] L. Wang, W. Dong, Y. Xu, Synthesis and characterization of hydroxypropyl methylcellulose and ethyl acrylate graft copolymers, Carbohydr. Polym. 68 (4) (2007) 626–636, https://doi.org/10.1016/j.carbpol.2006.07.031.
[64] C.J. Buchko, L.C. Chen, Y. Shen, D.C. Martin, Processing and microstructural characterization of porous biocompatible protein polymer thin films, Polymer 40 (26) (1999) 7397–7407, https://doi.org/10.1016/S0032-3861(98)00866-0.
[65] R. Inai, M. Kotaki, S. Ramakrishna, Structure and properties of electrospun PLLA single nanofibres, Nanotechnology 16 (2) (2005) 208–213, https://doi.org/10.1088/0957-4484/16/2/005.
[66] X. Wang, H. Chen, Z. Luo, X. Fu, Preparation of starch nanoparticles in water in oil microemulsion system and their drug delivery properties, Carbohydr. Polym. 138 (2016) 192–200, https://doi.org/10.1016/j.carbpol.2015.11.006.
[67] B. Carletto, J. Berton, T.N. Ferreira, L.F. Dalmolin, K.S. Paludo, R.M. Mainardes, P. V. Farago, G.M. Favero, Resveratrol-loaded nanocapsules inhibit murine melanoma tumor growth, Colloids Surf. B: Biointerfaces 144 (2016) 65–72, https://doi.org/10.1016/j.colsurfb.2016.04.001.
[68] W. Wu, X. Kong, C. Zhang, Y. Hua, Y. Chen, X. Li, Fabrication and characterization of resveratrol-loaded gliadin nanoparticles stabilized by gum Arabic and chitosan hydrochloride, LWT 129 (2020) 109532, https://doi.org/10.1016/j.lwt.2020.109532.
[69] H. Akinosho, S. Hawkins, L. Wicker, Hydroxypropyl methylcellulose substituent analysis and rheological properties, Carbohydr. Polym. 98 (1) (2013) 276–281, https://doi.org/10.1016/j.carbpol.2013.05.081.
[70] K.L.A. Chan, S.G. Kazarian, Detection of trace materials with Fourier transform infrared spectroscopy using a multi-channel detector, Analyst 131 (1) (2006) 126–131, https://doi.org/10.1039/b511243e.
[71] K.A. Ansari, P.R. Vavia, F. Trotta, R. Cavalli, Cyclodextrin-based nanosponges for delivery of resveratrol: in vitro characterisation, stability, cytotoxicity and permeation study, AAPS PharmSciTech 12 (1) (2011) 279–286, https://doi.org/10.1208/s12249-011-9584-3.
[72] Y.C. Lin, S.C.S. Hu, P.H. Huang, T.C. Lin, F.L. Yen, Electrospun resveratrol-loaded polyvinylpyrrolidone/cyclodextrin nanofibers and their biomedical applications, Pharmaceutics 12 (6) (2020) 1–16, https://doi.org/10.3390/pharmaceutics12060552.
[73] SpectraBase, Resveratrol - Optional[FTIR] - Spectrum - SpectraBase, Wiley, 2022. https://spectrabase.com/spectrum/2WyucMZRe67.
[74] G.B. Gonzales, G. Smagghe, C. Grootaert, M. Zotti, K. Raes, J. Van Camp, Flavonoid interactions during digestion, absorption, distribution and metabolism: A sequential structure-activity/property relationship-based approach in the study of bioavailability and bioactivity, Drug Metab. Rev. 47 (2) (2015) 175–190, https://doi.org/10.3109/03602532.2014.1003649.
[75] X. Zhou, Q. Ruan, Z. Ye, Z. Chu, M. Xi, M. Li, W. Hu, X. Guo, P. Yao, W. Xie, Resveratrol accelerates wound healing by attenuating oxidative stress-induced impairment of cell proliferation and migration, Burns 47 (1) (2021) 133–139, https://doi.org/10.1016/j.burns.2020.10.016.
[76] Š. Zupančič, Z. Lavrič, J. Kristl, Stability and solubility of trans-resveratrol are strongly influenced by pH and temperature, Eur. J. Pharm. Biopharm. 93 (2015) 196–204, https://doi.org/10.1016/j.ejpb.2015.04.002.
[77] S. Chessa, H. Huatan, M. Levina, R.Y. Mehta, D. Ferrizzi, A.R. Rajabi-Siahboomi, Application of the dynamic gastric model to evaluate the effect of food on the drug release characteristics of a hydrophilic matrix formulation, Int. J. Pharm. 466 (1–2) (2014) 359–367, https://doi.org/10.1016/j.ijpharm.2014.03.031.
[78] D.T. Pham, T.L. Nguyen, D.X.T. Nguyen, M.Q. Nguyen, T.P. Hau, N. Van Ky, V. De Tran, Swellable mucoadhesive hydroxypropyl methylcellulose microparticles incorporating ibuprofen for the local treatment of inflammatory diseases in the oral cavity, Journal of Applied Pharmaceutical Science 13 (11) (2023) 57–64, https://doi.org/10.7324/JAPS.2023.145863.
[79] J. Siepmann, H. Kranz, R. Bodmeier, N.A. Peppas, HPMC-matrices for controlled drug delivery: A new model combining diffusion, swelling, and dissolution mechanisms and predicting the release kinetics, Pharm. Res. 16 (11) (1999) 1748–1756, https://doi.org/10.1023/A:1018914301328.
[80] A. Smeets, R. Koekoekx, C. Clasen, G. Van den Mooter, Amorphous solid dispersions of darunavir: comparison between spray drying and electrospraying, Eur. J. Pharm. Biopharm. 130 (2018) 96–107, https://doi.org/10.1016/j.ejpb.2018.06.021.
[81] B.J. Lee, S.G. Ryu, J.H. Cui, Formulation and release characteristics of hydroxypropyl methylcellulose matrix tablet containing melatonin, Drug Dev. Ind. Pharm. 25 (4) (1999) 493–501, https://doi.org/10.1081/DDC-100102199.
[82] N.N. Vrettos, C.J. Roberts, Z. Zhu, Gastroretentive technologies in tandem with controlled-release strategies: A potent answer to oral drug bioavailability and patient compliance implications, Pharmaceutics 13 (10) (2021) 1591, https://doi.org/10.3390/pharmaceutics13101591.
[83] A. Amri, J.C. Chaumeil, S. Sfar, C. Charrueau, Administration of resveratrol: what formulation solutions to bioavailability limitations? J. Control. Release 158 (2) (2012) 182–193, https://doi.org/10.1016/j.jconrel.2011.09.083.
[84] C.C. Koga, J.E. Andrade, M.G. Ferruzzi, Y. Lee, Stability of trans-resveratrol encapsulated in a protein matrix produced using spray drying to UV light stress and simulated gastro-intestinal digestion, J. Food Sci. 81 (2) (2016) C292–C300, https://doi.org/10.1111/1750-3841.13176.
[85] M. Jo, C. Ban, K.K.T. Goh, Y.J. Choi, Enhancement of the gut-retention time of resveratrol using waxy maize starch nanocrystal-stabilized and chitosan-coated

Pickering emulsions, Food Hydrocoll. 112 (May 2020) (2021) 106291, https://doi.org/10.1016/j.foodhyd.2020.106291.
[86] C. Pu, W. Tang, M. Liu, Y. Zhu, Q. Sun, Resveratrol-loaded hollow kafirin nanoparticles via gallic acid crosslinking: an evaluation compared with their solid and non-crosslinked counterparts, Food Res. Int. 135 (April) (2020) 109308, https://doi.org/10.1016/j.foodres.2020.109308.
[87] R. Nunes, A. Baião, D. Monteiro, J. das Neves, B. Sarmento, Zein nanoparticles as low-cost, safe, and effective carriers to improve the oral bioavailability of resveratrol, Drug Deliv. Transl. Res. 10 (3) (2020) 826–837, https://doi.org/10.1007/s13346-020-00738-z.
[88] L. Qin, Y. He, X. Zhao, T. Zhang, Y. Qin, A. Du, Preparation, characterization, and in vitro sustained release profile of resveratrol-loaded silica aerogel, Molecules 25 (12) (2020), https://doi.org/10.3390/molecules25122752.
[89] L. Qin, X. Zhao, Y. He, H. Wang, H. Wei, Q. Zhu, T. Zhang, Y. Qin, A. Du, Preparation, characterization, and in vitro evaluation of resveratrol-loaded cellulose aerogel, Materials 13 (7) (2020) 1–12, https://doi.org/10.3390/ma13071624.
[90] S. Yara, J.C. Lavoie, J.F. Beaulieu, E. Delvin, D. Amre, V. Marcil, E. Seidman, E. Levy, Iron-ascorbate-mediated lipid peroxidation causes epigenetic changes in the antioxidant defense in intestinal epithelial cells: impact on inflammation, PLoS One 8 (5) (2013) e63456, https://doi.org/10.1371/journal.pone.0063456.
[91] Y. Fan, Y. Zhang, W. Yokoyama, J. Yi, Endocytosis of corn oil-caseinate emulsions in vitro: impacts of droplet sizes, Nanomaterials 7 (11) (2017), https://doi.org/10.3390/nano7110349.
[92] S. Guo, Y. Liang, L. Liu, M. Yin, A. Wang, K. Sun, Y. Li, Y. Shi, Research on the fate of polymeric nanoparticles in the process of the intestinal absorption based on model nanoparticles with various characteristics: size, surface charge and pro-hydrophobics, J. Nanobiotechnol. 19 (1) (2021) 32, https://doi.org/10.1186/s12951-021-00770-2.
[93] A. Acevedo-Fani, H. Singh, Biophysical insights into modulating lipid digestion in food emulsions, Prog. Lipid Res. 85 (2022) 101129, https://doi.org/10.1016/j.plipres.2021.101129.
[94] J.R. Han, L.P. Gu, R.J. Zhang, W.H. Shang, J.N. Yan, D.J. McClements, H.T. Wu, B. W. Zhu, H. Xiao, Bioaccessibility and cellular uptake of β-carotene in emulsion-based delivery systems using scallop (Patinopecten yessoensis) gonad protein isolates: effects of carrier oil, Food Funct. 10 (1) (2019) 49–60, https://doi.org/10.1039/c8fo01390j.
[95] J.H. Chung, J.S. Lee, H.G. Lee, Resveratrol-loaded chitosan–γ-poly(glutamic acid) nanoparticles: optimization, solubility, UV stability, and cellular antioxidant activity, Colloids Surf. B: Biointerfaces 186 (November 2019) (2020) 110702, https://doi.org/10.1016/j.colsurfb.2019.110702.
[96] Y. Fan, Y. Liu, L. Gao, Y. Zhang, J. Yi, Improved chemical stability and cellular antioxidant activity of resveratrol in zein nanoparticle with bovine serum albumin-caffeic acid conjugate, Food Chem. 261 (November 2017) (2018) 283–291, https://doi.org/10.1016/j.foodchem.2018.04.055.
[97] C. Pozo, S. Rodríguez-Llamazares, R. Bouza, L. Barral, J. Castaño, N. Müller, I. Restrepo, Study of the structural order of native starch granules using combined FTIR and XRD analysis, J. Polym. Res. 25 (12) (2018) 1–8, https://doi.org/10.1007/s10965-018-1651-y.
[98] Sigma-Aldrich, *IR Spectrum Table*. Sigma-Aldrich. https://www.sigmaaldrich.com/PT/en/technical-documents/technical-article/analytical-chemistry/photometry-and-reflectometry/ir-spectrum-table.
[99] P.M. Silva, C. Gonçalves, L.M. Pastrana, M.A. Coimbra, A.A. Vicente, M. A. Cerqueira, Recent advances in oral delivery systems of resveratrol: foreseeing their use in functional foods, Food Funct. 14 (23) (2023) 10286–10313, https://doi.org/10.1039/D3FO03065B.